Article

Institution of MECHANICAL ENGINEERS
Journal of AEROSPACE ENGINEERING

Proc IMechE Part G:
J Aerospace Engineering
2021, Vol. 0(0) 1–15

DOI: 10.1177/0954410021996491
journals.sagepub.com/home/pig
SAGE

A path planning model of a tiltrotor for approaching an aircraft carrier during landing

Yu Wu[1], Haixu Li[2] and Xichao Su[3]

Abstract

A path planning model concerning a tiltrotor approaching an aircraft carrier is established in this study. In the model, the characteristic of the tiltrotor, the landing task, and the environment of the carrier are taken into account. First, the motion equations and the maneuverability of the tiltrotor in each flight mode are presented, and the constraints of control variables and flight envelope are given. The returning flight of the tiltrotor is divided into three phases corresponding to the three flight modes of the tiltrotor, and the constraints in each phase and the goal are set. Considering the flight safety of the tiltrotor, the environment of the carrier is described as flyable space and no-fly zones, and the no-fly zones are set taking the influences of turbulence and wind field induced by the moving aircraft carrier into account. The path planning issue is formulated into an optimization problem under the constraints of control variables and state variables. According to the characteristic of the established model, a pigeon inspired optimization (PIO)-based path planning algorithm is developed integrating the "step-by-step" and "one effort" path search strategies. Simulation results demonstrate that the tiltrotor can reach the target point with a reasonable landing path. Comparison among different algorithms is also conducted to verify that the PIO algorithm is capable of solving this online path planning problem.

Keywords

Path planning, tiltrotor, aircraft carrier, multiple flight modes, pigeon inspired optimization

Date received: 23 February 2020; accepted: 28 January 2021

Introduction

Fixed-wing aircraft and helicopters are two typical types of aircraft. They have their own advantages in executing different tasks due to their different flight characteristics. Fixed-wing aircraft can fly with fast speed, and a helicopter is a kind of VTOL (short for vertical take-off and landing) aircraft. A tiltrotor is a special type of aircraft with three flight modes, that is, the airplane mode, the tilt mode, and the helicopter mode, which integrate the advantages of fixed-wing aircraft and helicopters,[1] and the transition among different flight modes is realized by changing the tilt angle of the nacelle.[2] In view of the above advantages, a tiltrotor is suitable for transportation, search, and logistic support both in military and civil use.[3] The tilt mode is the main weakness of a tiltrotor, which may lead to accidents in the process of changing its attitudes.[4] To ensure the flight safety, in many cases, the tiltrotor keeps on a level flight in the tilt mode.[5] The research studies related to path planning of a tiltrotor focus on the flight envelope determination[6] and the motion simulation.[7] For example, a novel hybrid single–multiple shooting method is developed in Ref. [8] to estimate the H–V (height–velocity) diagram of a tiltrotor. In Ref. [9], the turning trajectory of a tiltrotor under a single flight mode is obtained, and the results under the tilt mode and the airplane mode are compared. These studies provide the basics of exploring the maneuverability and motion of a tiltrotor, but the constraints of control variables in each flight mode still need to be further studied in the path planning problem for a tiltrotor.

The aircraft carrier is a busy and dynamic environment for tiltrotor landing.[10,11] Complex wind field caused by the motion of the carrier and the sea state has an influence on the flight safety of a tiltrotor.[12,13] The study on the path planning problem for VTOL aircraft landing on the carrier has not been reported so far. Similar studies focus on the

[1] College of Aerospace Engineering, Chongqing University, Chongqing, China
[2] Systems Engineering Research Institute, China State Ship building Corporation, Beijing, China
[3] Naval Aviation University, Yantai, China

Corresponding author:
Yu Wu, College of Aerospace Engineering, Chongqing University, No. 174, Shazheng Street, Shapingba District, Chongqing 400044, China.
E-mail: cquwuyu@cqu.edu.cn

path planning problem for an unmanned helicopter landing on a moving platform.[14,15] The landing process of a helicopter is described, and piecewise linear programming and Hamiltonian variational principle are applied to track the movement of the platform and generate the landing paths. The idea of dividing the landing task into several phases is a good way to deal with the problem, and the characteristic of multiple flight modes and the environment near the carrier must be considered in the path planning problem for the tiltrotor landing on the carrier.

When the tiltrotor is introduced on the carrier, it must execute specific tasks with other types of aircraft together. In the landing task, the landing area of the tiltrotor must be determined considering the working area of other aircraft. Besides, dynamical environment of the carrier also has an influence on the landing task, which increases the difficulty of obtaining a reasonable landing path. Moreover, a reasonable landing path for the tiltrotor is of great significance to improve the landing efficiency of different types of aircraft and ensure the normal operation on the busy flight deck.

In this study, a new path planning model is proposed to describe the task of the tiltrotor landing on the carrier, and the characteristics of the tiltrotor, landing task, and environment near the carrier are formulated into mathematical forms. To be specific, the motion equations of the tiltrotor are established, and the maneuverability and the flight envelope of the tiltrotor in each flight mode are given. The landing task is divided into three phases corresponding to the three flight modes of the tiltrotor, and the constraints in each landing phase and the goal of the landing task are proposed. Considering the busy and dynamic environment of the carrier, no-fly zones are set, which contain the spaces influenced by turbulence and wind field induced by the moving carrier. The path planning issue is formulated into an optimization problem under the constraints of control variables and state variables. Based on the characteristic of the established model, path search strategies integrating the pigeon inspired optimization (PIO) algorithm are designed for each landing phase. The PIO algorithm is a swarm intelligence-based algorithm and was first proposed by Duan in 2014.[16] The swarm intelligence-based algorithms have been widely applied in the path planning problem, and the advantage is to find a satisfactory solution within limited elapsed time,[17,18] which meets the requirement of an online planning problem. The validity of the PIO algorithm has been proved in the path planning problem,[19] and the PIO algorithm has demonstrated a better performance compared with other algorithms like genetic algorithm (GA) and particle swarm optimization (PSO) algorithm.[20] However, there are random parameters in the PIO algorithm, and in those studies the statistical characteristic is still underexplored which is important to evaluate the performance of the PIO algorithm. Besides, the computation time of the PIO algorithm also should be investigated to verify whether it is suitable for the online planning problem. The major contributions of this study are summarized as follows:

1. The motion model for tiltrotor path planning is established. Compared to existing studies, the multiple flight modes of the tiltrotor described by motion equations, maneuverability, and flight envelope are focused on. The transition conditions between different flight modes are also highlighted.
2. A path planning model for the tiltrotor approaching the carrier is developed. In this model, the whole landing task is divided into three phases corresponding to the three flight modes of the tiltrotor, and the constraints by category and the goals in each phase of the landing task are presented.
3. A PIO-based algorithm with the "step-by-step" and "one effort" search strategies is proposed considering the characteristic of each phase of the landing task, and a reasonable landing path for the tiltrotor is obtained. The proposed path planning algorithm is suitable for solving this problem after comparing with several other algorithms.

Description of the landing procedures of the tiltrotor

The task of the tiltrotor landing on the carrier specified in this study is defined as follows: When the moving carrier receives the information that there are aircraft returning, it will sail toward a certain direction with a constant velocity.[21] As the tiltrotor is usually far away from the carrier, it must fly with high speed to reduce the distance between the tiltrotor and the carrier. The airplane mode is applied to follow the motion of the carrier at a safe altitude above the carrier, and then the tiltrotor will decrease its altitude to land on the specified area of the flight deck with the minimum terminal error. The landing procedures of the tiltrotor can be divided into three phases.

Target pursuit

The tiltrotor flies with the airplane mode in this phase. It is required to track the movement of the carrier at a safe altitude and minimize the distance between them because flying at a low altitude will encounter more no-fly zones which would endanger the safety of the tiltrotor. When the horizontal distance is reduced to a certain value, this phase ends.

Stable transition

In this phase, the tiltrotor flies with the tilt mode. The tiltrotor tilts the nacelles, keeps on a level flight, and gets closer to the target point. As the tilt mode is hard to be handled, the prime goal is to ensure the flight safety and make the transition finished as soon as possible, and the nacelles are tilted continuously from the airplane mode to

the helicopter mode.[22] Note that this phase is ended after the nacelles have been tilted to 90°.

Final descent

The tiltrotor flies with the helicopter mode in this phase, and the carrier moves toward a fixed direction according to the instruction from the commander (e.g. attacking the enemy), which can make the landing process easier. In this study, the target point is set right above the specified landing position on the flight deck. The reasons are as follows. In real environment, the specified landing position changes with the motion of the carrier, and the accurate motion model of the carrier is usually obtained by prediction.[23] The path between the target point and the specific landing position is decided by the motion of the carrier and need not to be planned. In engineering, the landing controller is developed to ensure that the tiltrotor can land at the specified position on the flight deck.[24]

To make a better understanding of the above landing procedures, the diagram of the tiltrotor returning is shown in Figure 1.

In Figure 1, the flight modes corresponding to the landing phases are shown. The tiltrotor needs to transit the flight mode twice before it reaches the moving target point. The task of path planning is to generate the path for each landing phase and guarantee that the tiltrotor reaches the target point accurately and safely. The goal of each landing phase is presented in Table 1.

Mathematical model of the path planning problem

In this section, the conceptual model is abstracted first to present the idea of solving the problem. Then, considering the multiple flight modes of the tiltrotor, the motion model is given, and the maneuverability and the flight envelope of the tiltrotor under each flight mode are defined. The busy and dynamic environment of the carrier is described by flyable space and no-fly zones. The constraints in each phase of the landing task are proposed, and the goal of landing task is set as the weighted sum of three items.

Conceptual model of the path planning problem

In Section 2, the whole landing task of the tiltrotor has been divided into three phases, which provides a frame of solving the problem. On this basis, the conceptual model is built to organize the idea of solving the problem, as shown in Figure 2.

In Figure 2, path planning is closely related to the tiltrotor, the landing task, and the environment of the carrier, and it is formulated into an optimization problem including the motion equations, the constraints of control variables and state variables, and the cost function. The dotted lines with double arrows denote that the flight mode corresponds to the landing phase. According to the characteristic of each landing phase, different strategies are developed to generate the path. After the path is

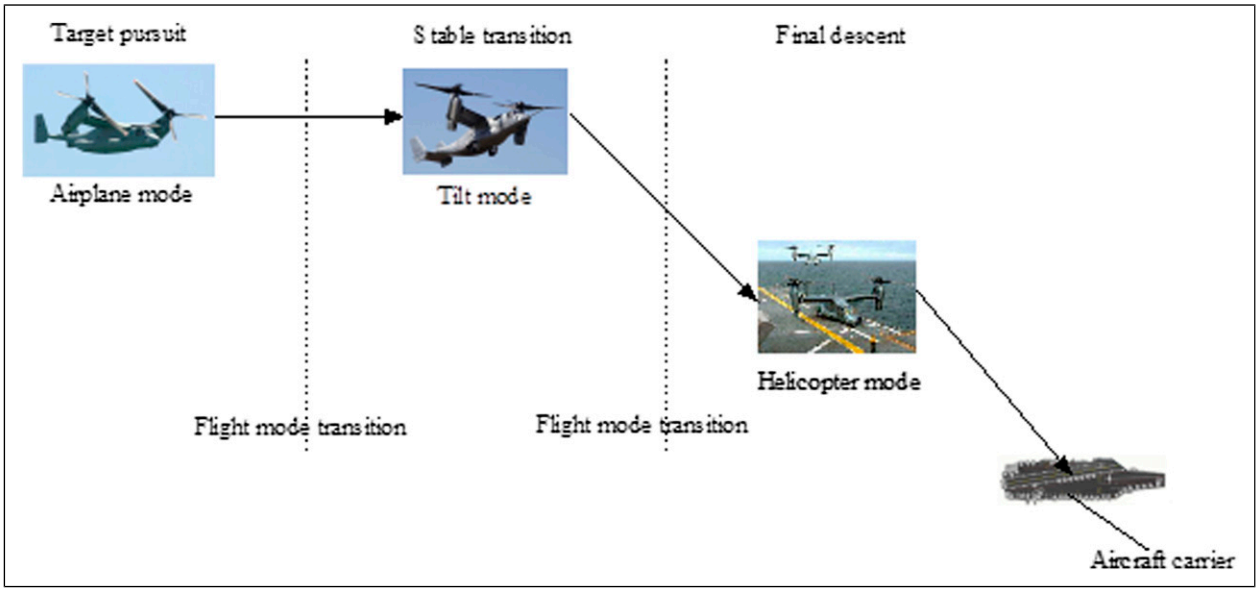

Figure 1. The three phases of the tiltrotor returning the carrier.

Table 1. Description of each flight mode of the tiltrotor and each landing phase.

Landing phase	Flight mode	Goal
Target pursuit	Airplane	Get close to the carrier
Stable transition	Tilt	Transit the flight mode quickly and safely
Final descent	Helicopter	Reach the target point

obtained, the performance of the path planning algorithm is analyzed to explain its rationality.

Motion model of the tiltrotor

To describe the motion of the tiltrotor, two coordinate systems are defined, as shown in Figure 3.

In Figure 3, OXYZ is defined as the ground frame, which is fixed on the ground. The origin O is defined as the initial position of the target point, and the axis OX points at the direction which the carrier sails. The axis OZ is vertically downward, and the axis OY can be determined by the right hand rule. $O_kX_kY_kZ_k$ is the kinetic frame which originates at the center of gravity of the tiltrotor. α, ϕ, γ, and φ are the angle of attack, bank angle, flight path angle, and yaw angle, respectively, and V denotes the flight velocity of the tiltrotor. T, L, and D are the thrust, lift force, and drag force, and δ is the tilt angle of the nacelle. It can be seen from Figure 3 that $\delta = 0^o$ and $\delta = 90^o$ correspond to the airplane mode and the helicopter mode, respectively. The motion model of the tiltrotor can be expressed as follows[9]

$$\dot{x} = V \cos\gamma \cos\varphi \tag{1}$$

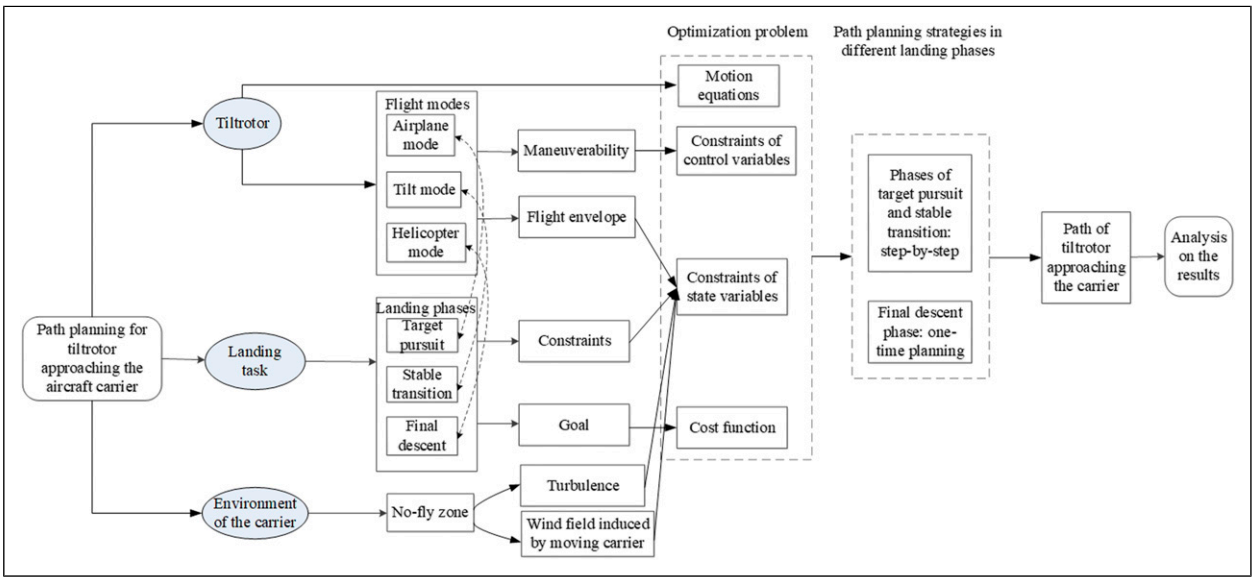

Figure 2. Conceptual model of the path planning problem.

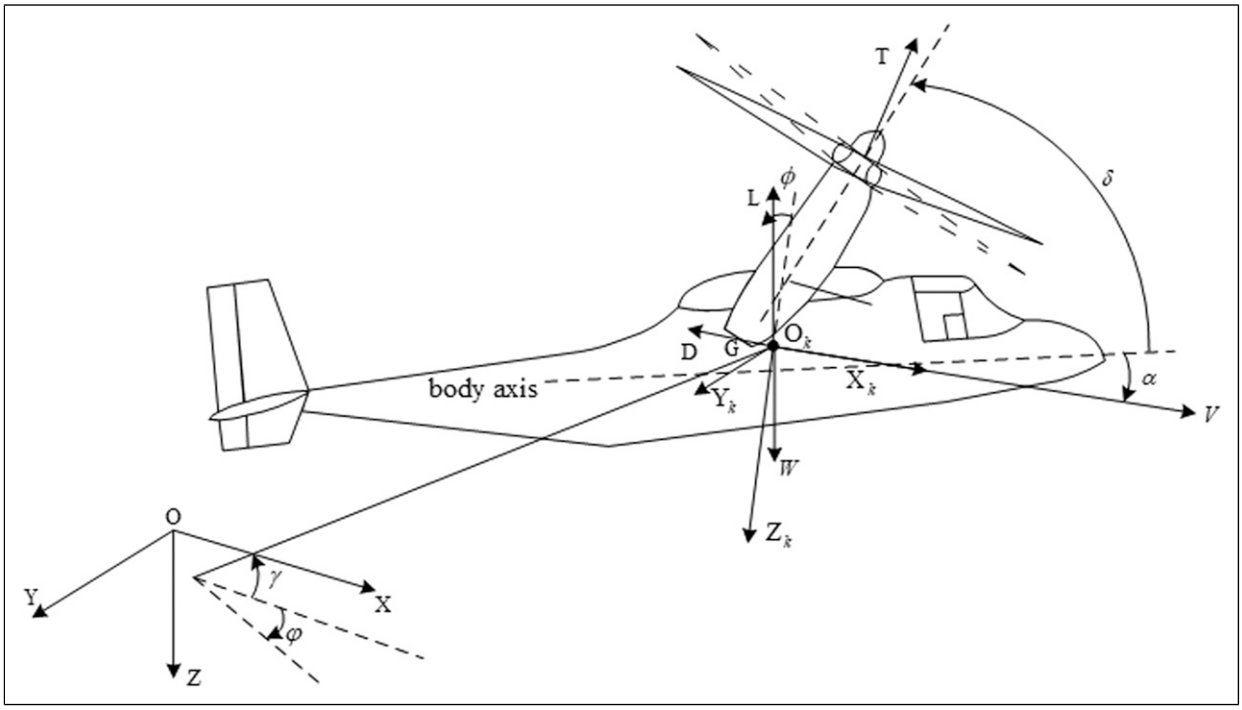

Figure 3. Description of motion of the tiltrotor.

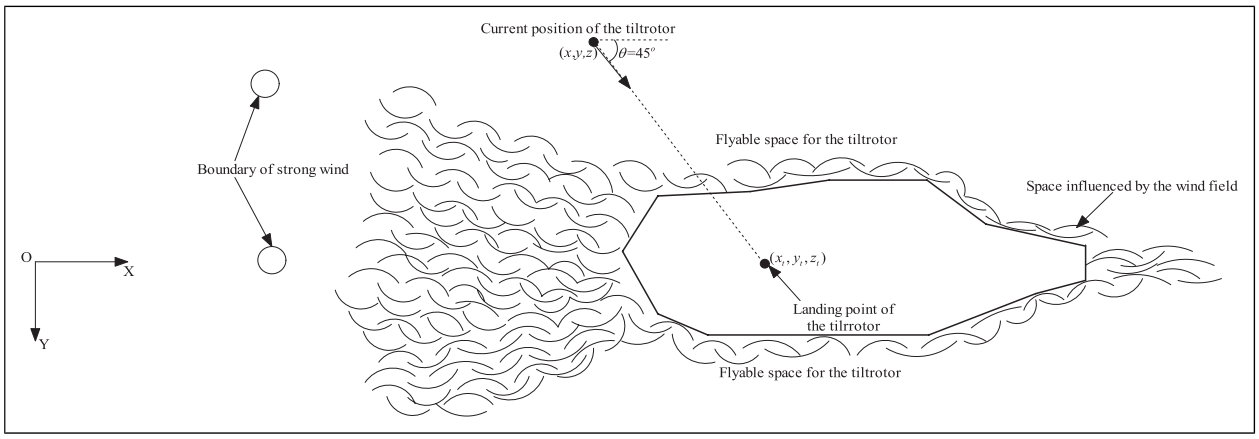

Figure 4. Description of the space near the carrier.

$$\dot{y} = V\cos\gamma\sin\varphi \tag{2}$$

$$\dot{z} = -V\sin\gamma \tag{3}$$

$$\dot{V} = \frac{[T\cos(\alpha+\delta) - D]}{m} - g\sin\gamma \tag{4}$$

$$\dot{\gamma} = \frac{[T\sin(\alpha+\delta)\cos\phi + L\cos\phi]}{(mV)} - \frac{g\cos\gamma}{V} \tag{5}$$

$$\dot{\varphi} = \frac{[T\sin(\alpha+\delta)\sin\phi + L\sin\phi]}{(mV\cos\gamma)} \tag{6}$$

$$\dot{\delta} = l \tag{7}$$

From equations (1)–(7), (x, y, z) is the position of the center of gravity of the tiltrotor in the ground frame, and l is the tilt rate of the nacelle. In this problem, the state variables can be denoted as the vector $\boldsymbol{x} = [x \quad y \quad z \quad V \quad \gamma \quad \varphi \quad \delta]$, and the control variables are $\boldsymbol{u} = [\alpha \quad \phi \quad P \quad l]$, where p is the engine power. Besides, the forces T, D, and L in equations (4)–(6)– can be calculated by the following equations

$$T = \eta\frac{P}{V} \tag{8}$$

$$D = \frac{1}{2}\rho V^2 S C_D \tag{9}$$

$$L = \frac{1}{2}\rho V^2 S C_L \tag{10}$$

where η is the efficiency coefficient, ρ is the atmospheric density, and S is the reference area of the tiltrotor. C_L and C_D are the lift and drag coefficients.

Modeling of the no-fly zone

The no-fly zone is set to guarantee the flight safety of the tiltrotor. The tiltrotor must avoid the wind field induced by the moving carrier and turbulence. The description of the no-fly zone is shown in Figure 4.

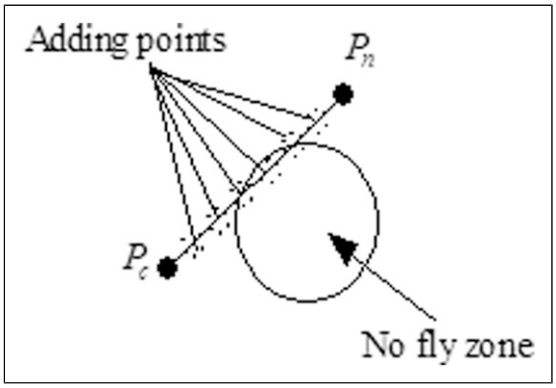

Figure 5. Strategy of no-fly zone detection.

In Figure 4, the space near the carrier is divided into several parts. The tiltrotor can only fly in the flyable space, and other spaces are set as the no-fly zones. The no-fly zones contain the space influenced by the wind field, that is, the wind field induced by the moving carrier and the turbulence. Note that the constraint of the direction of reaching the target point for the tiltrotor is also presented in Figure 4, and the details will be described in Section 3.4.

Considering that the weather changes rapidly on the sea, turbulence (strong wind) may occur in some places, and the tiltrotor must avoid those spaces to ensure the flight safety. The space of turbulence is described as cylinders with finite height, and they are the fixed space relative to the ground frame. Assuming that the current position of the tiltrotor is P_c and the next possible path point is P_n which is given by the path planning algorithm, the strategy of judging whether the tiltrotor has entered the no-fly zone is shown in Figure 5.

In Figure 5, a certain number of points are added between P_c and P_n, and their positions are determined by linear interpolation and can be denoted as $P_i^{add}(x_i, y_i, z_i)$ (i=1,2,…, q), where q is the number of added points. Note that P_c and P_n are not in the no-fly zone, but the points in the path segment P_cP_n need to be further checked to ensure the flight safety. Although some feasible space may be abandoned using this strategy, it guarantees that the

tiltrotor can judge the no-fly zone in advance, and there may be not enough time for the tiltrotor close to the no-fly zone to avoid due to the constraint of maneuverability. Assume that the boundaries of cylinders satisfy the equations $f_j(x, y, z) = 0$ (j=1,2,…, p), where p is the number of cylinders. If the following equation is met, the tiltrotor is regarded as falling into the space of turbulence

$$\begin{cases} (x_i - x_{oj})^2 + (y_i - y_{oj})^2 \le R_j^2 \\ \quad and \\ z_{j\min} \le z_i \le z_{j\max} \end{cases} \tag{11}$$

where (x_{oj}, y_{oj}) and R_j are the center and the radius of circle corresponding to cylinder j and z_{jmin} and z_{jmax} are the height range of cylinder j. The proposed detection strategy gives an accurate judgment and can guarantee the flight safety of the tiltrotor.

Constraints in different landing phases

When the tiltrotor is approaching the carrier, the constraints of control variables and state variables must be imposed on each phase of the landing task. These constraints are described as follows.

Constraints of control variables. The control variables must vary within a certain range to satisfy the constraint of maneuverability. These constraints can be expressed as follows

$$\alpha_{min} \le \alpha \le \alpha_{max} \tag{12}$$

$$|\phi| \le \phi_{max} \tag{13}$$

$$P_{min} \le P \le P_{max} \tag{14}$$

Note that α_{min} is a small negative value, and α_{max} is a positive value that ensures the flight safety. The constraint of l is not presented here because it will vary according to the given law. The details are explained later.

Constraints of states of the tiltrotor in different phases of the landing task. In the landing task, the flight modes of the tiltrotor correspond to the landing phases, and the states of the tiltrotor must be changed within certain ranges according to the requirement of each landing phase. Next, the constraint of flight velocity is presented first, and other constraints are formulated in different landing phases.

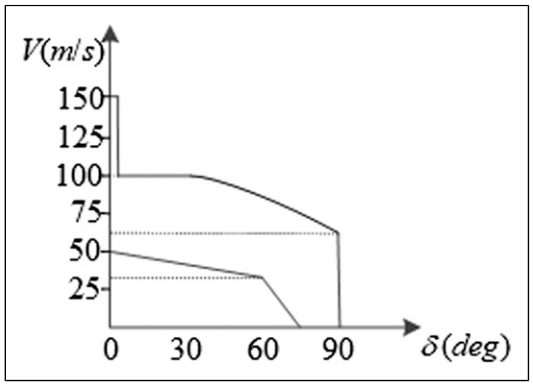

Figure 6. The flight envelope of the tiltrotor

In each flight mode, the tiltrotor must fly within a certain velocity range to ensure the flight safety. Figure 6 shows the relationship between the flight velocity range and the corresponding tilt degree of the nacelle,[3] which can be calculated by the dynamic model of the tiltrotor established in Ref. [25].

In Figure 6, δ is the tilt angle of the nacelle. When $\delta = 0^\circ$, the tiltrotor flies with the airplane mode, and the nacelle is parallel with the fuselage. When $\delta = 90°$, the helicopter mode is used, and the nacelle is perpendicular to the fuselage. The tilt mode is a transition mode in which the tile angle changes from 0° to 90° (or from 90° to 0°). Table 2 shows the range of flight velocity at some specific tilt angles of the nacelle.

Constraints in the target pursuit phase and the stable transition phase. In these two phases, the tiltrotor flies at a stable altitude, and fewer constraints are imposed on, as shown in Table 3.

$\gamma = 0^o$ means the tiltrotor flies at a fixed height. In the target pursuit phase, $\delta = 0^\circ$ guarantees that the tiltrotor flies with the airplane mode. In the stable transition phase, $\dot{\varphi} = 0^\circ/s$ makes the tiltrotor fly straightly, and $\dot{\delta} \ge 0^\circ/s$ ensures the continuity of flight mode transition. Note that the change law of $\dot{\delta}$ is regulated by δ according to the report from NASA,[26] in which the change law of $\dot{\delta}$ is tested to ensure the stability and safety of the tiltrotor during the transition process. The data are shown in Table 4.

Table 2. Examples of flight velocity range at different tilt angles of the nacelle.

$\delta(^o)$	0	30	60	75	90
V_{min} (m/s)	50	40	30	0	0
V_{max} (m/s)	150	100	85	76	70

Table 3. Constraints of states in the target pursuit phase and the stable transition phase.

Phase	Constraints
Target pursuit	$\gamma = 0°$; $\delta = 0°$
Stable transition	$\gamma = 0°$; $\dot{\varphi} = 0^\circ/s$; $\dot{\delta} \ge 0^\circ/s$

Table 4. The change law of $\dot{\delta}$ depending on δ.

δ(deg.)	0	2.5	3	10	20	30	40
$\dot{\delta}$(deg/s)	2.8	2.8	14	12.5	11.63	11.4	11.4
δ(deg)	50	60	70	80	87.5	88	90
$\dot{\delta}$(deg/s)	11.7	12.45	13.3	14.25	15	3	0

The value of δ at any moment during the flight mode transition can be obtained by fitting the data in Table 4, and it cost about 10 s to finish the transition process.

Constraints in the final descent phase. In the final descent phase, $\delta = 90^{o}$ must be always met to make sure that the tiltrotor flies with the helicopter mode. Besides, a number of terminal constraints must be obeyed to ensure the accuracy and safety of reaching the target point.

In the flyable space depicted in Figure 4, the tiltrotor is required to reach the target point within a certain range of angle to avoid the influence of the wind field. In Figure 4, the value of θ can be calculated by the following equation

$$\theta = \tan^{-1}\left(\frac{y_t - y}{x_t - x}\right) \tag{15}$$

where (x, y) and (x_t, y_t) are the positions of the tiltrotor and the target point in the ground frame, respectively. Note that the constraint of $\theta = 45^{\circ}$ is set based on the assumption that the carrier sails against the wind. In a real-world scenario, when there is crosswind acting on the carrier, asymmetric wind will lead to the asymmetry no-fly zones in the near space of the carrier. On this occasion, the wind graph is used to evaluate the maximum relative wind velocity and the landing direction for the helicopter under certain sea condition and environment, and the ideal value of θ will change according to the wind graph.[27]

Furthermore, the above constraint can be met on a condition that there is a limitation imposed on the value of yaw angle φ at the last several moments of landing. This is because the terminal value of θ (denoted as $\theta(t_f)$) is relevant to φ, and an appropriate limitation on φ can make the constraint of reaching the target point satisfied easier. This limitation imposed on φ can be written as follows

$$0^{\circ} \le \varphi(t) \le 90^{\circ} \tag{16}$$

Finally, the following constraints must be obeyed to ensure the accuracy and safety of the landing task

$$e_x = \left|x(t_f) - x_f\right| \le e_{xmax} \tag{17}$$

$$e_y = \left|y(t_f) - y_f\right| \le e_{ymax} \tag{18}$$

$$e_z = \left|z(t_f) - z_f\right| \le e_{zmax} \tag{19}$$

$$e_\theta = \left|\theta(t_f) - \theta_f\right| \le e_{\theta max} \tag{20}$$

$$e_{V_x} = \left|V_x(t_f) - V\right|_c \le e_{V_x max} \tag{21}$$

where t_f is the terminal moment, e is the terminal error of each item, and e_{max} is the maximum terminal error permitted. Equations (17)–(19)– are set to make the terminal error of each direction fall into a small range. Equation (20) regulates the maximum error of the angle of reaching the target point. In equation (21), V_x is the component of V along the axis OX which can be calculated by equation (1), and V_C is the velocity of the carrier. As the carrier always sails along the axis OX, V_x should be as close as V_C because the tiltrotor and the carrier must be relatively still to make the landing controller perform better.

Cost function of path planning

As mentioned before, the goal is to reduce the distance between the tiltrotor and the target point and adjust the flight velocity to translate into the next flight mode, and the smoothness of the path is of relevance for the comfort considerations of manned operations. The corresponding cost function can be written as

$$J = \omega_1 \cdot ||P_{tilt} - P_{tar}|| + \omega_2 \cdot V + \omega_3 \cdot \int_{t_0}^{t_f} \left(\dot{\gamma}^2 + \dot{\varphi}^2\right) dt \tag{22}$$

The first item denotes the distance between the tiltrotor and the target point. t_0 and t_f are the starting time and terminal time of flight. ω_1, ω_2, and ω_3 are the adjustable weights of each item, respectively, considering that the main objective is not exactly the same in each landing phase. For example, the distance between the tiltrotor and the target point must be reduced in the target pursuit phase and the stable transition phase, and the final flight velocity of the tiltrotor in each flight mode must fall into the range shown in Figure 6 to translate into the next flight mode successfully. ω_1 is set as a larger value in the initial target pursuit phase to pay more attention to the distance, and ω_2 becomes more important in the final target pursuit phase to ensure that the flight velocity meet the constraint of the tilt mode.

Path planning algorithm for the tiltrotor approaching the carrier

In this section, different path search strategies are designed considering the characteristic of the landing task and the established model. In different landing phases, the path can be obtained in a step-by-step way or in one effort. Then, the principle of the PIO algorithm is introduced and is integrated into the path search strategies. The procedures of the algorithm are also presented, and how the constraints can be met in the path planning algorithm is shown.

Search strategies in different landing phases

The tiltrotor flies in a dynamic environment and has different goals in each landing phase. Different search strategies are proposed to cope with the situations.

Strategy in the target pursuit phase and the stable transition phase. The distance between the tiltrotor and the target point is far in these two phases, and the tiltrotor must avoid the no-fly zones. To adapt to the changing environment, only the motion of the tiltrotor in a short time window of future (denoted as T_w) will be planned in one step of search to ensure the flight safety. Assume that the discrete time interval is Δt, and the number of path point (denoted as

N_w) which can be determined in one step of search is $T_w/\Delta t$. The cost function in equation (22) can be expressed as the form in equation (23)

$$J^{t_C} = \omega_1 \cdot \left|\left|P_{tilt}^{t_C+T_w} - P_{tar}^{t_C+T_w}\right|\right| + \omega_2 \cdot V^{t_C+T_w} + \omega_3 \cdot \int_{t_C}^{t_C+T_w} \left(\dot{\gamma}^2 + \dot{\varphi}^2\right) dt \tag{23}$$

where $P_{tilt}^{t_C+T_w}$ and $P_{tar}^{t_C+T_w}$ are the positions of the tiltrotor and the target point at the moment $t_c + T_w$. $V^{t_C+T_w}$ is the flight velocity of the tiltrotor at the moment $t_c + T_w$, and J^{t_C} is the cost function at the current moment t_c.

Strategy in the final descent phase. In this phase, the distance between the tiltrotor and the target point is relatively small, and the nearby environment is known to provide a reliable condition to land. Therefore, the rest unplanned path can be obtained in one effort. Note that if the value of a control variable at every moment is optimized, the computation load will be heavy, and it may not meet the demand of online planning. Different from the search strategy in other two landing phases, the collocation points (distributed uniformly, denoted as t_k, and the number of the collocation points is N_c) are chosen, which means that only the control variables at those time points are optimized, and the values of control variables at other time points (denoted as $t_i(t_k < t_i < t_{k+1})$) can be obtained by linear interpolation, as expressed in equations (24)–(26)

$$\alpha_{t_i} = \frac{\alpha_{t_{k+1}} - \alpha_{t_k}}{t_{k+1} - t_k} \cdot (t_i - t_k) + \alpha_{t_k} \tag{24}$$

$$\phi_{t_i} = \frac{\phi_{t_{k+1}} - \phi_{t_k}}{t_{k+1} - t_k} \cdot (t_i - t_k) + \phi_{t_k} \tag{25}$$

$$P_{t_i} = \frac{P_{t_{k+1}} - P_{t_k}}{t_{k+1} - t_k} \cdot (t_i - t_k) + P_{t_k} \tag{26}$$

In equation (24), when the values of α_{t_k} and $\alpha_{t_{k+1}}$ are determined, the value of α_{t_i} can be calculated. The same is true for the control variable ϕ_{t_i} and P_{t_i} in equations (25) and (26).

Description of the pigeon inspired optimization algorithm and the application in the path planning problem

To make a better understanding of the PIO algorithm, the mathematical formulations of the two operators in the algorithm, that is, the map and compass operator and the landmark operator, will be presented, and the background of the PIO algorithm is omitted in this study considering that those contents can be seen in many references. How the PIO algorithm is integrated into the path planning problem is also highlighted at the end of this section.

The map and compass operator. In the algorithm, each pigeon i has its position X_i and velocity V_i, and the position and velocity are both D-dimension vectors according to the scale of problem. For example, N_{w1}, N_{w2}, and N_c are the dimensions of the vector in each landing phase. In each iteration, the position X_i and velocity V_i can be updated with the following equations

$$V_i^{t+1} = V_i^t \cdot e^{-R(t+1)} + rand \cdot \left(X_g - X_i^t\right) \tag{27}$$

$$X_i^{t+1} = X_i^t + V_i^{t+1} \tag{28}$$

Where t is the times of iteration, R is the operator factor, *rand* is a uniform random number in the interval [0,1], and X_g is the current global best position. In the second item of equation (27), the position is actually divided by the time step which equals to 1. The same is true for the second item in equation (28), and the time step is omitted. In equation (27), R determines the degree that velocity of a pigeon inherits that of the last generation, and the step size of updating the velocity of each pigeon is decided by *rand*, which is variable in each time of iteration in equation (28).

Landmark operator. In the landmark operator, the number of pigeons is decreased by half in each iteration. The center of pigeons' positions is referenced in the landmark operator. Suppose the center of the pigeons' positions at the tth iteration is X_c^t, the rule of updating the position for pigeon i can be expressed as the following equations

$$N_P^t = \frac{N_P^{t-1}}{2} \tag{29}$$

$$X_c^t = \frac{\sum X_i^t \cdot fitness\left(X_i^t\right)}{N_P^t \sum fitness\left(X_i^t\right)} \tag{30}$$

$$X_i^{t+1} = X_i^t + rand \cdot \left(X_c^t - X_i^t\right) \tag{31}$$

where N_P^t is the number of pigeons at the tth iteration, *fitnesss* $\left(X_i^t\right)$ is the fitness value of pigeon i, which can be calculated by equation (22) according to the different landing phases, and *rand* is a uniform random number in the interval [0,1]. Similar to the uniform random number in equation (27), here *rand* represents the step size of updating the position of each pigeon.

Note that after the position is updated according to equations (28) and (31), the values of control variables may not meet the constraints proposed from equations (12)–(14). To make the normal running of the algorithm, the values of control variables which violate the constraints are set as the closest threshold, respectively. When the pigeons' positions are updated by the two operators, the current global best position X_g will be updated after comparing the fitness values, and the pigeon corresponding to the smallest fitness value is regarded as X_g.

To sum up, a two-step position updating strategy is used in the PIO algorithm. In the map and compass operator, the pigeons update their positions referring to the current velocity and the global best position, which is similar to the mechanism in the PSO algorithm. In the landmark operator, half of all the pigeons with the worst

fitness values are abandoned, which can accelerate the convergence rate. Besides, pigeons update their positions referring to the center of all pigeons rather than the global best position, which avoids trapping into the local optimum. All those characteristics make PIO algorithm superior to other similar swarm intelligence-based algorithms.

As mentioned in Section 4.1, different search strategies are used in different landing phases, and the procedures of searching the path can be summarized as the flow chart as presented in Figure 7.

In Figure 7, path search strategy No. 1 is applied in the first two landing phases, and path search strategy No. 2 is used in the last phase to obtain the remaining unplanned path in one effort. The PIO algorithm is adopted in both of the two strategies to search the path.

In the initialization, the values of control variables are fetched within their ranges, and the corresponding fitness value can be calculated by equation (22). In each iteration, after the position of each pigeon is updated using equations (28) or (31), each solution will be checked to judge whether it satisfies all the constraints formulated in equation (11) and equations (16)–(21). If one or more constraints are violated, the corresponding fitness value (the cost function in equation (22)) will be set to a large value (usually a lager order of magnitude than the normal value) to indicate that the solution is infeasible and will be abandoned.

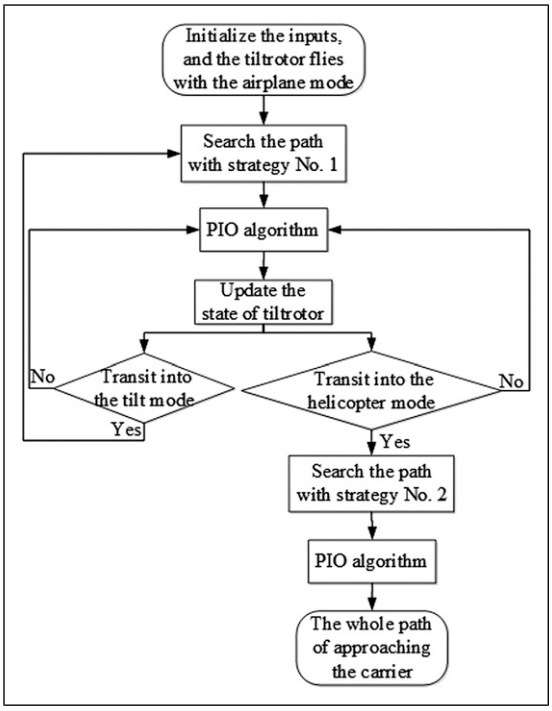

Figure 7. The procedures of the path planning algorithm.

Table 5. Parameters settings in motion equations of the tiltrotor (1SHP = 735 N m/s).

Parameter	α_{min}	α_{max}	ϕ_{max}	P_{min}	P_{max}	η	S
Value	−3°	18°	30°	62.5SHP	1250SHP	0.8	15.21 m^2

Simulation results

To investigate the validity of the established model and the PIO-based path planning algorithm to solve the path planning problem of the tiltrotor approaching the carrier, simulations using the parameters of the tiltrotor XV-15[28] are conducted. All the results are obtained by running different methods on a desktop computer with Intel Core i7-3370 3.40 GHz with MATLAB R2016b.

The starting point of the tiltrotor and the target are set as (−4000, −3000, −1000) and (0,0,0), respectively, and the carrier always moves toward the axis OX with the velocity of V_c=10 m/s. The parameter settings regarding the motion model of the tiltrotor are shown in Table 5, and the aerodynamic parameter is referred to Ref. [9].

Besides, the parameters ω_1, ω_2, and ω_3 in the cost function (equation (22)) are set different values in each landing phase. In the phases of target pursuit and stable transition, ω_1 and ω_2 are set as 0.5 and 0.2, respectively, as it is more important for the tiltrotor to approach the carrier. While in the phase of final descent, to reduce the impact with the flight deck becomes increasingly important, and ω_1 and ω_2 are set as 0.3 and 0.4, respectively. In the three landing phases, ω_3 is always set to 0.3 to pay attention to the smoothness of the path to some extent.

The parameters used in the PIO algorithm are set according to the scale of the problem and are based on Refs. [16] and [19]. To result in the best performance, the parameters are determined by trial and error, as presented in Table 6. The constraints of the terminal errors are given in Table 7.

Results of path planning with the PIO-based method

With the above settings, the results of path planning are obtained using the proposed method. The approaching path is presented in Figure 8, and the states of the tiltrotor are shown in Figure 9.

In these two figures, the curves with different colors present different flight modes of the tiltrotor, and the tiltrotor spent most of flight time in the helicopter mode. The tiltrotor flies at a fixed altitude (the height is 1000 m

Table 6. Parameters setting in the pigeon inspired optimization algorithm.

Parameter	N_{w1}	N_{w2}	N_C	N_p	R	N_{c1}	N_{c2}
Value	5	1	64	100	0.2	20	30

Table 7. Constraints of terminal errors.

Error	$e_{\theta max}$	$e_{V_x max}$	e_{xmax}	e_{ymax}	e_{zmax}
Value	5°	1 m/s	0.1 m	0.1 m	2 m

from the sea level) and changes the direction in the airplane mode, and then it translates into the tilt mode. In the tilt mode, the tiltrotor kept a level flight without changing the direction to make the transition safe, which is consistent with the green line segments in the second and the third subgraph of Figure 9. In the helicopter mode, the tiltrotor makes a detour in the OXY plane because the flight time in the OZ axis is longer than that in the OXY plane. The tiltrotor has to fly more distance to wait the displacement of the OZ axis to reach the specified altitude. The values of terminal states of the tiltrotor are listed in Table 8.

The symbol "—" means that there is no desired value about this item. In Table 8, the terminal error of each item

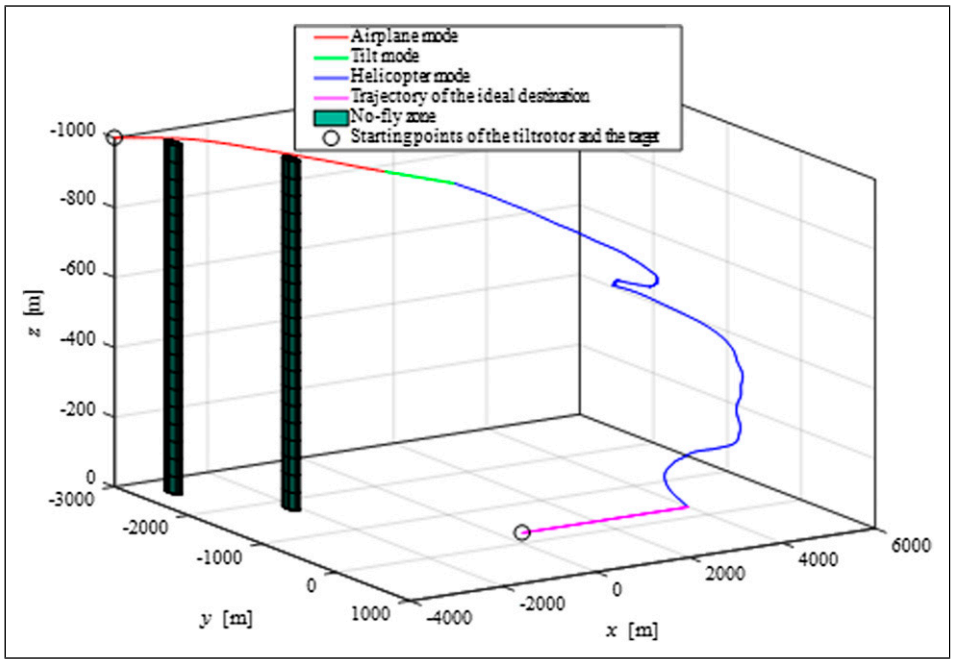

Figure 8. Landing path of the tiltrotor and motion of the target point.

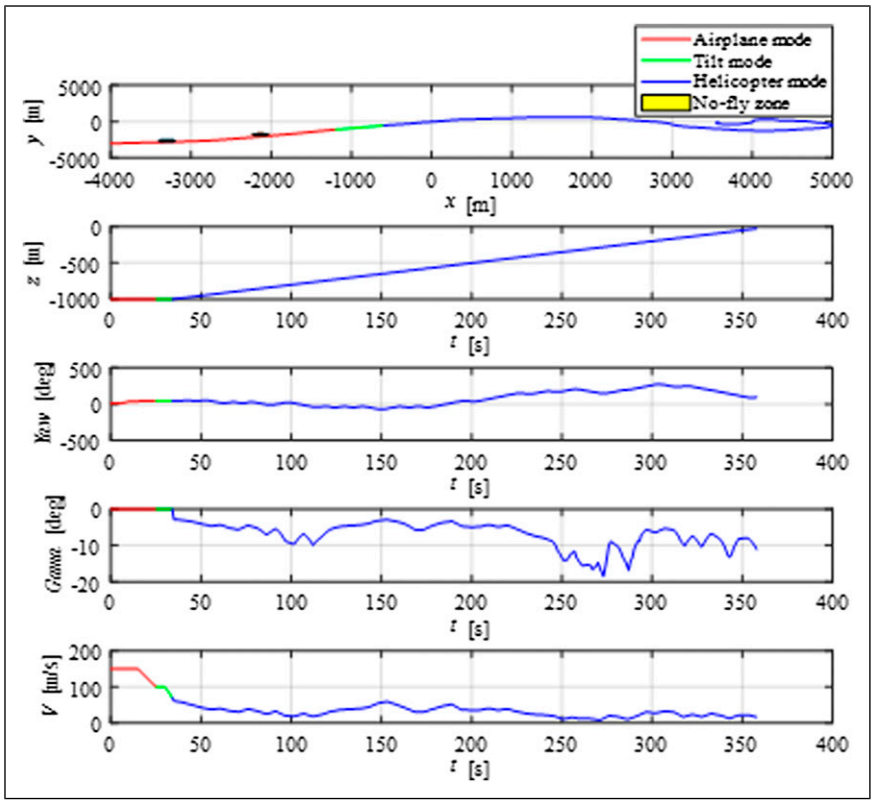

Figure 9. The states of the tiltrotor during flight.

Table 8. Actual and desired terminal states of the tiltrotor.

Value	*x(m)*	*y(m)*	*z(m)*	*φ(rad)*	*γ(rad)*	V_x*(m/s)*	*θ(deg)*
Actual	3573.08	−0.075	−30	1.653	−0.193	10.7	42.06
Desired	3573	0	−30	—	—	10	45

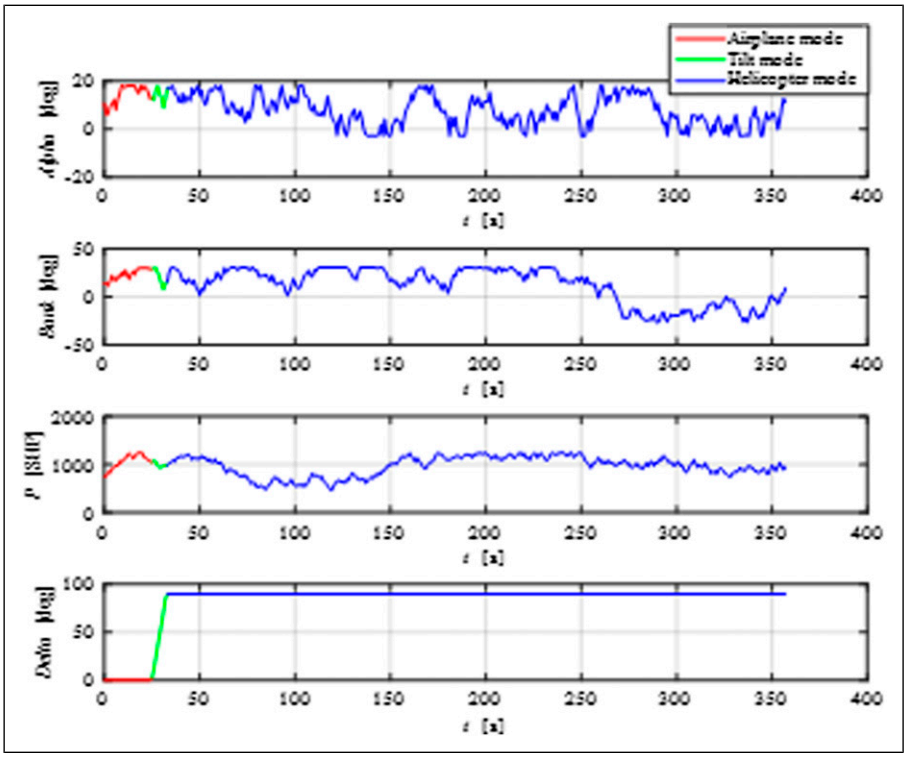

Figure 10. Variation of control variables.

meets the constraints listed in Table 7. Finally, the variation of control variables is shown in Figure 10.

It can be seen that the control variables vary within the ranges given in Table 5, and the tilt angle of the nacelle changes from 0^o to 90^o during the flight. Note that the variation curves of control variables in Figure 10 are not so smooth as only the smoothness of flight states is considered in the cost function expressed by equation (22). The oscillation of control variables can be removed by fitting the curve before practical application. The above results demonstrate that the tiltrotor can reach the moving target point over the carrier with slight deviation, and the generated path satisfies various constraints.

Comparison among PIO, PSO, and GA algorithms

To further investigate the performance of the PIO-based method solving the path planning problem for the tiltrotor approaching the carrier, the PSO algorithm and GA algorithm are also used to solve the same problem. The parameters of PSO and GA are consulted to Refs. [29] and [30], respectively, and other settings of experiments are the same with those listed in Tables 5–7. As PIO, PSO, and GA are population-based algorithms, there are random numbers when generating new solutions. To make a comprehensive comparison, each of the three algorithms is run 50 times independently, and the best results and the statistical results are presented below.

The best results among the 50 times of running are shown in Figures 11 and 12. As the path in the target pursuit stage and the stable transition stage is generated step by step, Figure 11 shows the fitness value of each step. In general, the three lines are almost coincident due to the large value range of the y axis. To make it clearer, some important data in Figure 11 are given in Table 9.

The fitness value decreases as the step number increases because the tiltrotor got closer to the target point over time. Note that the fitness value of step No. 5 is smaller than that of the later steps because at the end of the target pursuit phase, ω_2 becomes larger in equation (23) to ensure that the tiltrotor satisfies the constraint of the flight envelope before it translates into the tilt mode. In Table 9, the fitness values of the three population-based algorithms do not make a big difference.

Figure 12 shows the fitness values of the three different algorithms in the final descent phase, and the PIO algorithm has the fastest convergence rate. To obtain more information from Figure 12, Table 10 presents the convergence times and the final fitness value of each algorithm.

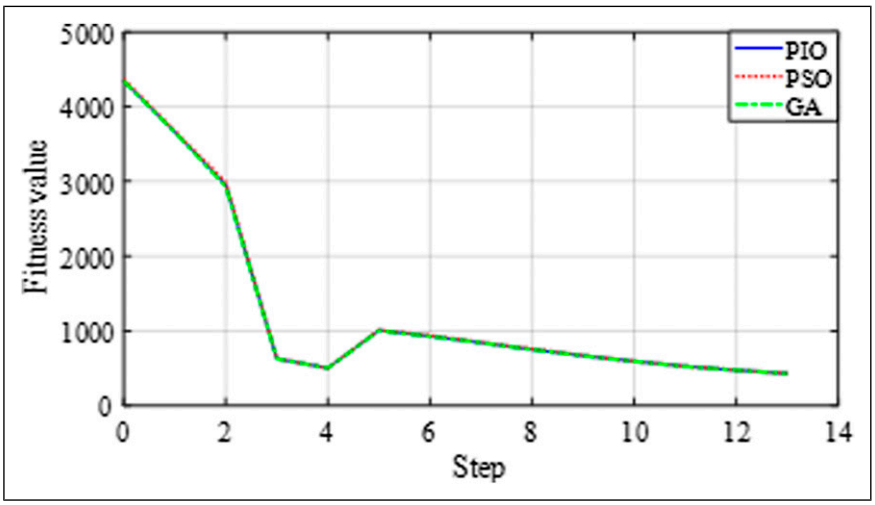

Figure 11. Fitness value of each step (target pursuit phase and stable transition phase).

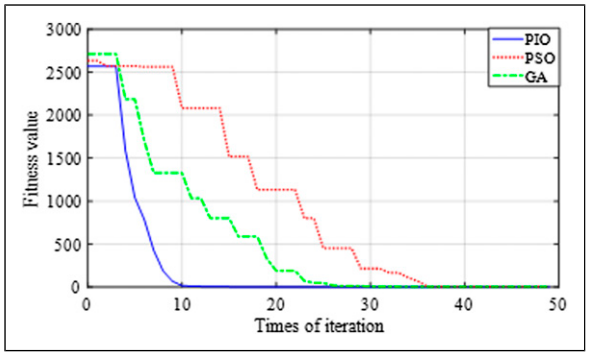

Figure 12. Fitness value of the final step with the time of iteration (final descent phase).

Table 9. Fitness value of some steps in Figure 11.

Step No.	*1 (10^3)*	*5 (10^2)*	*9 (10^2)*	*13 (10^2)*
PIO	4.3578	5.0663	7.5814	4.7693
PSO	4.3834	5.1200	7.7017	4.8383
GA	4.3683	5.2127	7.6828	4.9187

Note: PIO: pigeon inspired optimization; PSO: particle swarm optimization; GA: genetic algorithm.

Table 10. Fitness value of some steps in Figure 12.

Algorithm	*PIO*	*PSO*	*GA*
Convergence times	22	40	35
Final fitness value	2.648	2.747	2.704

Note: PIO: pigeon inspired optimization; PSO: particle swarm optimization; GA: genetic algorithm.

The convergence time in Table 10 means the fitness value becomes convergent after certain times of iterations. It can be concluded from Tables 9 and 10 that PIO, PSO, and GA have similar results. The PIO algorithm has the fastest convergence rate and can converge within 22 times of iteration. The paths obtained by the three different algorithms are shown in Figure 13. In the target pursuit phase and the stable transition phase, the landing paths do not show a big difference because in the "step-by-step" path search strategy, the number of optimized control variable is small in each step. In the final descent phase, with different algorithms, different landing paths are shown to reach the target point.

Next, statistical results on computation time and fitness value will be given to further explain the performance of each algorithm solving this problem, as shown in Tables 11 and 12.

In Table 11, "1" and "2" denote the target pursuit phase and the stable transition phase, respectively, and "C" and "F" present computation time and fitness value. Among the three algorithms, the PIO algorithm spends the least time on computation. Besides, the PIO algorithm results in the best solution and the most stable performance. The time complexity of the three population-based algorithms is analyzed to explain the reason why PIO has the fastest computation speed.

In Table 13, D is the dimension of solution, T is the times of iteration, and T_1 and T_2 are the times of iteration of the two operators in the PIO algorithm ($T = T_1 + T_2$). The initialization of solution is dealt with only once in computing, and only the items in bold are taken into account in determining the time complexity of the algorithm. In this problem, the dimension of solution in each stage of the landing task is $D_1 = 5$, $D_2 = 1$, and $D_3 = 64$, respectively. With the data in Table 6, the time complexity of each algorithm when solving the problem can be calculated, as shown in Table 14.

The time complexity of PIO is the least among the three population-based algorithms in each phase, which can explain the results in Tables 11 and 12. Note that, in Table 11, the maximum computation time of the PSO algorithm is shorter than that of GA in the stable transition phase, which does not conform to the conclusion shown in Table 14. This is because the time complexity of the two algorithms does not show a big difference in the stable transition phase, and the insufficient running times of the

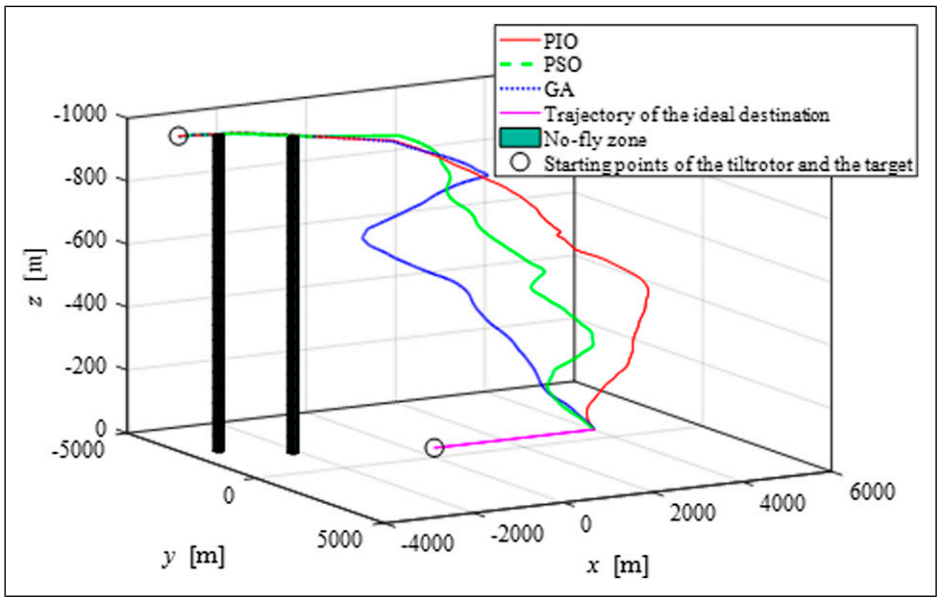

Figure 13. Landing paths of the tiltrotor using three different algorithms.

Table 11. Statistical results on computation time of each step in the target pursuit phase and the stable transition phase.

	Minimum		*Maximum*		*Mean*		*Std*	
	1 (10^{-3})	2 (10^{-4})	1 (10^{-3})	2 (10^{-4})	1 (10^{-3})	2 (10^{-4})	1 (10^{-4})	2 (10^{-5})
PIO	2.7	7.0	7.6	9.1	5.3	7.8	3.7	7.7
PSO	3.6	7.5	8.0	9.4	6.3	8.7	4.1	8.2
GA	3.4	7.3	7.9	9.5	6.1	8.5	4.2	8.3

Note: PIO: pigeon inspired optimization; PSO: particle swarm optimization; GA: genetic algorithm.

Table 12. Statistical results on computation time and fitness value in the final descent phase.

	Best		*Worst*		*Mean*		*Std*	
	C(10^{-2})	F	C(10^{-2})	F	C(10^{-2})	F	C(10^{-4})	F(10^{-3})
PIO	3.1	2.648	8.5	2.961	5.8	2.753	5.1	7.7
PSO	5.7	2.747	12.3	3.158	9.6	2.932	5.7	8.1
GA	4.4	2.704	9.1	3.026	6.6	2.834	6.6	9.2

Note: PIO: pigeon inspired optimization; PSO: particle swarm optimization; GA: genetic algorithm.

Table 13. The complexity analysis of PIO, PSO, and GA.

Step	*PIO*	*PSO*	*GA*
Initialize position	$N_p \times D$	$N_p \times D$	$N_p \times D$
Initialize velocity	$N_p \times D$	$N_p \times D$	—
Calculate fitness value	N_p	N_p	N_p
Update velocity	$N_p \times D$	$N_p \times D$	—
Calculate new position	$N_p \times D$	$N_p \times D$	—
Cross over	—	—	$N_p/2$
Variation	—	—	$N_p \times D$
Calculate fitness value	N_p	N_p	N_p
Calculate the solution center	$N_p/2 \times D$	—	—
Calculate new position	$N_p/2 \times D$	—	—
Calculate fitness value	$N_p/2$	—	—
Time complexity	$T_1(N_p + 2N_p \times D) + N_p(1-0.5^{T}{}_2) + 2N_p \times D(1-0.5^{T}{}_2)$	$T(N_p + 2N_p \times D)$	$T(1.5N_p + N_p \times D)$

Note: PIO: pigeon inspired optimization; PSO: particle swarm optimization; GA: genetic algorithm.

Table 14. The time complexity of PIO, PSO, and GA when solving the problem.

Time complexity	*Phase 1*	*Phase 2*	*Phase 3*
PIO	23,100	6300	270,900
PSO	55,000	15,000	645,000
GA	32,500	12,500	327,500

Note: PIO: pigeon inspired optimization; PSO: particle swarm optimization; GA: genetic algorithm.

algorithms lead that the result of one simulation does not conform to the statistical results. To sum up, the PIO algorithm shows its superiority in convergence rate and computation time in the path planning problem for the tiltrotor approaching the carrier, and a reasonable solution also can be obtained.

Conclusions

A new path planning model is developed in this study to deal with the path planning problem for the tiltrotor approaching the carrier.

The established model is essentially different from the previous path planning models. First of all, the motion equations and maneuverability of the tiltrotor in each flight mode are considered, and the flight envelope and the constraints of control variables are given. Second, considering the requirement of the landing task, the returning flight of the tiltrotor is divided into three phases corresponding to the three flight modes, and the constraints of each phase and the goal are proposed. Additionally, no-fly zones are set considering the environment of carrier, that is, the influences of turbulence and wind field. Finally, the path planning problem is formulated into an optimization problem under the constraints of control variables and state variables, and the goal is denoted as the weighted sum of distance between the tiltrotor and the target point, the flight velocity of the tiltrotor, and the smoothness of path.

Considering the characteristic of the established model, the step-by-step strategy and the one effort strategy are developed and are applied in different landing phases, and the PIO algorithm is integrated into the strategies to generate the path. The rationality of the developed path planning model is verified in a typical landing task, and the PIO algorithm is suitable for solving this online planning problem through the comparison with other algorithms in convergence rate, solution quality, and computation time using the statistical approach.

In the future, further investigation on the accuracy of model is needed. First, a more complicated dynamic model of the tiltrotor would be established to describe the motion with higher dimensions, which will add more constraints as more factors will be involved. The computing time of solving the flight states of the tiltrotor also will be increased as the number of nonlinear differential equations becomes greater. Both are new challenges when designing the path planning algorithm. Moreover, the strength of the wind field near the carrier needs to be calculated considering the motion of the carrier, the sea state, and the aerodynamic configuration of the tiltrotor.

Declaration of conflicting interests

The author(s) declared no potential conflicts of interest with respect to the research, authorship, and/or publication of this article.

Funding

The author(s) disclosed receipt of the following financial support for the research, authorship, and/or publication of this article: This research work is financially supported by the Chongqing Research Program of Basic Research and Frontier Technology with the grant number of cstc2020jcyj-msxmX0602 and Fundamental Research Funds for the Central Universities with the project reference number of 2020CDJ-LHZZ-066.

ORCID iD

Yu Wu https://orcid.org/0000-0002-9319-9498

References

1. Liu Z, He Y, Yang L, et al. Control techniques of tilt rotor unmanned aerial vehicle systems: a review. *Chin J Aeronautics* 2017; 30(1): 135–148.
2. Wang Z, Gong Z, Chen Y, et al. Practical control implementation of tri-tiltrotor flying wing unmanned aerial vehicles based upon active disturbance rejection control. *Proc Inst Mech Eng G: J Aerospace Eng* 2020; 234(4): 943–960.
3. Zhang J, Yu W and Qu X. A trajectory planning model of tiltrotor considering multi-phase and multi-mode flight. *Proc Inst Mech Eng Part G: J Aerospace Eng* 2019; 233(16): 6019–6031.
4. Chen C, Zhang J, Zhang D, et al. Control and flight test of a tilt-rotor unmanned aerial vehicle. *Int J Adv Robotic Syst* 2017; 14(1): 1–12.
5. Zhang J, Sun L, Qu X, et al. Time-varying linear control for tiltrotor aircraft. *Chin J Aeronautics* 2018; 31(1): 632–642.
6. Santos MA, Cardoso DN, Rego BS, et al. A discrete robust adaptive control of a tilt-rotor UAV for an enlarged flight envelope. In: IEEE 56th annual conference on decision and control (CDC), Melbourne, Australia, 12–15 December 2017, pp. 5208–5214.
7. Shen J, Singleton JD, Piatak DJ, et al. Multibody dynamics simulation and experimental investigation of a model-scale tiltrotor. *J Am Helicopter Soc* 2016; 61(2): 1–11.
8. Bottasso CL, Luraghi F and Maisano G. Efficient rotorcraft trajectory optimization using comprehensive models by improved shooting methods. *Aerospace Sci Technology* 2012; 23(1): 34–42.
9. Miyamoto T, Takano H, Yamaguchi I, et al. A study on the trajectory optimization of a tiltrotor with the tilting rate limit. In: Asia-Pacific international symposium on aerospace technology, Shanghai, China, 1 January 2014.
10. Wu Y, Sun L and Qu X. A sequencing model for a team of aircraft landing on the carrier. *Aerospace Sci Technology* 2016; 54: 72–87.
11. Wu Y, Hu N and Qu X. A general trajectory optimization method for aircraft taxiing on flight deck of carrier. *Proc Inst Mech Eng Part G: J Aerospace Eng* 2019; 233(4): 1340–1353.

12. Guan Z, Ma Y, Zheng Z, et al. Prescribed performance control for automatic carrier landing with disturbance. *Nonlinear Dyn* 2018; 94(2): 1335–1349.
13. Zhou Z, Huang J and Yi M. Pruning operator for minimum deck wind in carrier aircraft launch. *Proc Inst Mech Eng Part G: J Aerospace Eng* 2020; 234(3): 655–664.
14. Saripalli S and Sukhatme GS. Landing a helicopter on a moving target. IEEE international conference on robotics and automation, Roma, Italy, 10–14 April 2007, 2030–2035.
15. Wu C, Qi J, Song D, et al. LP based path planning for autonomous landing of an unmanned helicopter on a moving-platform. *J Unmanned Syst Technology* 2013; 1(1): 7–13.
16. Sun Y, Duan H and Xian N. Fractional-order controllers optimized via heterogeneous comprehensive learning pigeon-inspired optimization for autonomous aerial refueling hose-drogue system. *Aerospace Sci Technology* 2018; 81: 1–13.
17. Wang X, Deng Y and Duan H. Edge-based target detection for unmanned aerial vehicles using competitive bird swarm algorithm. *Aerospace Sci Technology* 2018; 78: 708–720.
18. Sushnigdha G and Joshi A. Evolutionary method based integrated guidance strategy for reentry vehicles. *Eng Appl Artif Intelligence* 2018; 69: 168–177.
19. Zhao J and Zhou R. Pigeon-inspired optimization applied to constrained gliding trajectories. *Nonlinear Dyn* 2015; 82(4): 1–15.
20. Sun Y and Duan H. Pigeon-inspired optimization and lateral inhibition for image matching of autonomous aerial refueling. *Proc Inst Mech Eng Part G: J Aerospace Eng* 2018; 232(8): 1571–1583.
21. Chen C, Tan W-Q, Qu X-J, et al. A fuzzy human pilot model of longitudinal control for a carrier landing task. *IEEE Trans Aerospace Electron Syst* 2018; 54(1): 453–466.
22. Francesco GD and Mattei M. Modeling and incremental nonlinear dynamic inversion control of a novel unmanned tiltrotor. *J Aircraft* 2016; 53(1): 73–86.
23. Tan CK, Wang J, Paw YC, et al. Autonomous ship deck landing of a quadrotor using invariant ellipsoid method. *IEEE Trans Aerospace Electron Syst* 2016; 52(2): 891–903.
24. Moon J, Domercant JC and Mavris D. A simplified approach to assessment of mission success for helicopter landing on a ship. *Int J Control Automation Syst* 2015; 13(3): 680–688.
25. Li H, Qu X and Wang W. Multi-body motion modeling and simulation for tilt rotor aircraft. *Chin J Aeronautics* 2010; 23(4): 27–34.
26. Rosenstein H, Mcveigh MA and Mollenkof PAV. *STOL Tilt Rotor Aircraft Study Mathematical Model for a Real Time Simulation of a Tilt Rotor Aircraft*. *Calif NASA*, 8 1973, report No. CR114601.
27. Huang Y. *Research on Key Technology of Automatic Carrier Landing for Unmanned Helicopter*. Northwestern Polytechnical University, Dissertation, 2015.
28. Maisel MD, Giulianetti DJ and Dugan DC. *The history of the XV-15 tilt rotor research aircraft from concept to flight*. Washington, D. C.: Monographs in Aerospace History, 2000.
29. Shi Y and Eberhart RC. Parameter selection in particle swarm optimization. In: International conference on evolutionary programming, Berlin, Heidelberg, 25–27 March 1998, pp. 591–600.
30. Eberhart RC and Shi Y. Comparison between genetic algorithms and particle swarm optimization. In: International conference on evolutionary programming, Berlin, Heidelberg, 25–27 March 1998, pp. 611–616.